ACS OMEGA

http://pubs.acs.org/journal/acsodf

Article

Effect of Graphene Oxide and Temperature on Electrochemical Polymerization of Pyrrole and Its Stability Performance in a Novel Eutectic Solvent (Choline Chloride−Phenol) for Supercapacitor Applications

Hani K. Ismail,* Idrees B. Qader, Hasan F. Alesary, Jalil H. Kareem,* and Andrew D. Ballantyne

Cite This: https://doi.org/10.1021/acsomega.2c03882

Read Online

ACCESS | Metrics & More | Article Recommendations | Supporting Information

ABSTRACT: Polypyrrole (Ppy)-modified graphene oxide (GO) electrodes were synthesized for the first time in a choline chloride−phenol-based deep eutectic solvent at various temperatures via electrochemical methods without the addition of any inorganic or organic catalysts. The surface morphologies and structures of the modified films were assessed via scanning electron microscopy, transmission electron microscopy, Fourier transform infrared spectroscopy, and X-ray diffraction techniques. The electrochemical properties and stability of the modified electrodes were investigated via cyclic voltammetry and impedance spectroscopy at various temperatures and scan rates. The results showed that the specific capacitance of the nanocomposites decreased with increasing scan rate during cycling. Additionally, the specific capacitances of the pure Ppy and Ppy/GO films increased with increasing temperature of the electrolyte (monomer-free), attributed to the reduction in viscosity at elevated temperature. The specific capacitances at 5 mV s^{-1} were found to be 1071.78 and 594.79 F g^{-1} for Ppy/GO (20 wt %) at 50 and 25 °C, respectively. It was also observed that the resistance in the cell decreased with increasing electrolyte temperature. Ppy/GO at 50 mV s^{-1} was found to have the highest capacitance retention of 85% after 2000 cycles, showing better cycling stability than the pure Ppy film. Herein, the incorporation of GO in the Ppy matrix led to improved specific capacitance and cyclic stability, suggesting that Ppy/GO could represent a promising electrode material for supercapacitor applications.

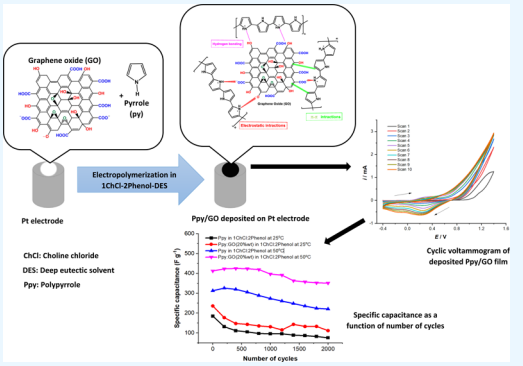

1. INTRODUCTION

Supercapacitors are a promising energy storage system for sustainable energy management due to their intrinsic properties, such as good cycle performance and reversibility, safety in operation, and high-power capability, ensuring that they have received a vast amount of attention.[1,2] The mechanism of charge storage in supercapacitors is classified into two categories: (i) pseudocapacitors (such as conducting polymers and metal oxides) and (ii) electronic double-layer capacitors (EDLCs) (such as carbonaceous materials). The charge storage efficiency in a pseudocapacitor is a result of chemical reactions based on the Faradaic process that take place through an activated substance component of the electrodes, while the efficiency of EDLCs (via non-Faradaic mechanisms) is a result of the separation of charges (ionic and electronic) between the solution and electrode interface.[2,3]

Conducting polymers such as polyaniline, polypyrrole (Ppy), poly(3,4-ethylenedioxythiophene), poly(3-methylthiophene), and poly(1,5-diaminoanthraquinone) have been extensively investigated with regard to their potential as pseudocapacitor materials[4] due to the possibility of utilizing them in various industrial applications including sensors, batteries, anti-corrosion materials, membranes, transducers, optical storage media, and electrochemical devices.[5] Typically, they are inexpensive and relatively easy to prepare in comparison with metal oxides and carbon-based substances. Among the various conducting polymers, Ppy is extensively applied in high-performance pseudocapacitors[6] due to its good physio-chemical properties such as its high electrical conductivity, rapid redox switching, biocompatibility, and environmental stability, as well as a large capacitance and high storage capacity. Consequently, various polymerization methods have been utilized for the preparation of Ppy with different morphologies via either electrochemical or chemical routes at the micrometric or nanometric scales.[7] However, most conducting polymers (including Ppy) have poor charge/discharge cycling stability, believed to be due to the variation

Received: June 21, 2022
Accepted: September 2, 2022

in volume of polymer during charge discharge. Swelling/shrinkage processes commonly occur during redox processes to enable the insertion/rejection of counterions. Internal stresses within the film cause deterioration, gradually causing a reduction in charge storage behavior.[8,9] It has been found that carbon-based materials such as graphene, carbon nanotubes, and activated carbons extensively interact with conjugative polymers to improve their cycling stability in electrochemical capacitors due to increased conductivity through the films and an increase in absorption sites. One of carbonaceous substances used in this field is graphene oxide (GO), which is a graphene derivative. In addition, its structure is disordered, rough, and predominantly amorphous, having a large quantity of functional groups (epoxy, hydroxyl, and carboxyl groups) on its surface, which can enhance the mechanical properties and cycling stability performance of polymer composites.[10] It has been demonstrated that cycling stability of pseudocapacitive processes can be enhanced by modification with carbon-based nanomaterials. Charge can be stored via Faradaic and non-Faradaic mechanisms in the modified electrodes, resulting in excellent specific capacitance and good electrochemical cycling stability.[11]

Many researchers have prepared conducting polymer composites in aqueous and organic electrolytes due mostly to their high conductivity and the fact that they facilitate mass transport.[12,13] However, there are limitations associated with the use of aqueous and organic electrolytes, such as their small potential windows and short lifetime stability, which can result in rapid degradation of the polymer in the electrolyte.[14,15] Recent works have studied the electrochemical polymerization of conducting polymer composites in ionic liquids (ILs)[16,17] due to their wide potential windows, which can improve the durability, thermal stability, and morphology of the deposited film.[18] However, the high cost and toxicity of ILs have limited their applicability.[19] Deep eutectic solvents (DESs) are formed when a significant depression of the melting point of a mixture is observed compared to those of the individual components.[20] Typically, these are mixtures of quaternary ammonium salts mixed with metal salts or hydrogen bond donors (HBDs),[21,22] although others such as the combination of metal salts with HBDs also exist.[23] DESs have been applied in many areas including electrodeposition of metals and alloys,[24,25] conducting polymers,[26,27] metal finishing, desulfurization,[28] pharmaceuticals,[29,30] and energy storage.[31] This is due to the fact that they are cheap, are easy to prepare, are non-volatile, are biodegradable, are insensitive to water, and typically have low toxicity, all of which make their use in large-scale applications highly favorable.[32,33] Several researchers have synthesized various conducting polymers in DESs and studied different associated parameters, including the growth mechanism and cycling stability of polymers in DESs as well as ion and solvent transport.[34−36] Indeed, the type of solvent and, thus, the size of the dopant counteranions have a significant effect on all the films' properties including structure, morphology, and cycling stability,[37,38] where the positive charges are produced in the backbone of polymer during oxidation. Thereafter, solvated anions ingress into the oxidized polymer matrix to counterbalance the positive charge. Resultingly, the mobility of anions and electrochemical stability are strongly dependent on the nature of the solvent and the types of species present.

The present work employs the novel electrochemical polymerization of pyrrole in a DES electrolyte, consisting of choline chloride (ChCl) and phenol in a 1:2 mol ratio. This DES is of interest as it can form a eutectic solvent at room temperature, possesses long-term stability at elevated temperatures, and is composed of affordable raw materials.[39] Most DESs contain aliphatic HBDs. The presence of phenolic rings as a component within the DES may result in modified deposition behavior of both Ppy and GO due to modified solvent−solute interactions. Resultingly, evaluation of Ppy films with/without GO deposited from this solvent in the application of supercapacitors is significant and has not, to date, been considered. Here, we grow and characterize electrolytic Ppy films grown in a 1ChCl:2Phenol DES with/without the presence of GO. Films have been deposited at different temperatures and concentrations of GO in the deposition medium using the cyclic voltammetry (CV) method. Ppy and Ppy/GO composites were transferred to background monomer-free electrolytes, and their electrochemical performance was evaluated using various potential windows, scan rates, and temperatures. The morphological features of the deposited polymers were characterized via scanning electron microscopy (SEM) and transmission electron microscopy (TEM). To confirm the incorporation of Ppy on the surface of GO, Fourier transform infrared (FTIR) spectroscopy and X-ray diffraction (XRD) techniques were used.

2. EXPERIMENTAL SECTION

2.1. Materials. Pyrrole monomer (C_4H_5N, 98%) and choline chloride ($C_5H_{14}ClNO$, ≥ 99.5%) were obtained from Sigma-Aldrich, while graphite (99%) used to prepare GO and phenol (C_6H_6O 99%) were obtained from Alfa Aesar and Thomas Bake. All materials were used without further purification.

2.2. Preparation of DES. In this work, a mixture of choline chloride (ChCl) and phenol was prepared in a 1:2 M ratio [e.g., ChCl (10 g) and phenol (13.5 g)] according to that used in previous work.[40] Then, the mixture was placed on a hot plate and heated to 40 °C with stirring using a magnetic stirrer until a homogeneous electrolyte was formed, as shown in Figure 1. In this study, 1ChCl:2Phenol DES was used as the

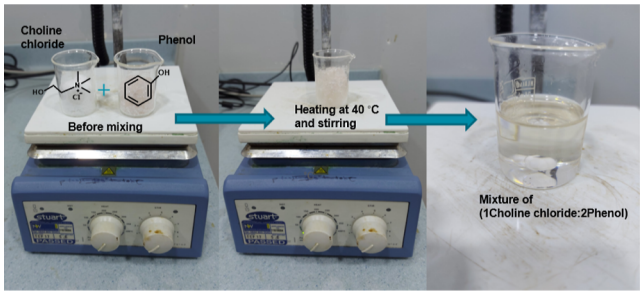

Figure 1. Photographs of preparation of DES electrolyte from choline chloride and phenol.

background electrolyte for the electropolymerization of pyrrole and as the cycling electrolyte when determining the electrochemical stability of the thin films. Conceptually, this DES may be regarded as mildly acidic due to the phenol present in the DES acting as a proton donor.

2.3. Synthesis of GO from Graphite. GO was synthesized from graphite powder according to a modified Hummers method. A detailed process for preparing GO was

https://doi.org/10.1021/acsomega.2c03882
ACS Omega XXXX, XXX, XXX−XXX

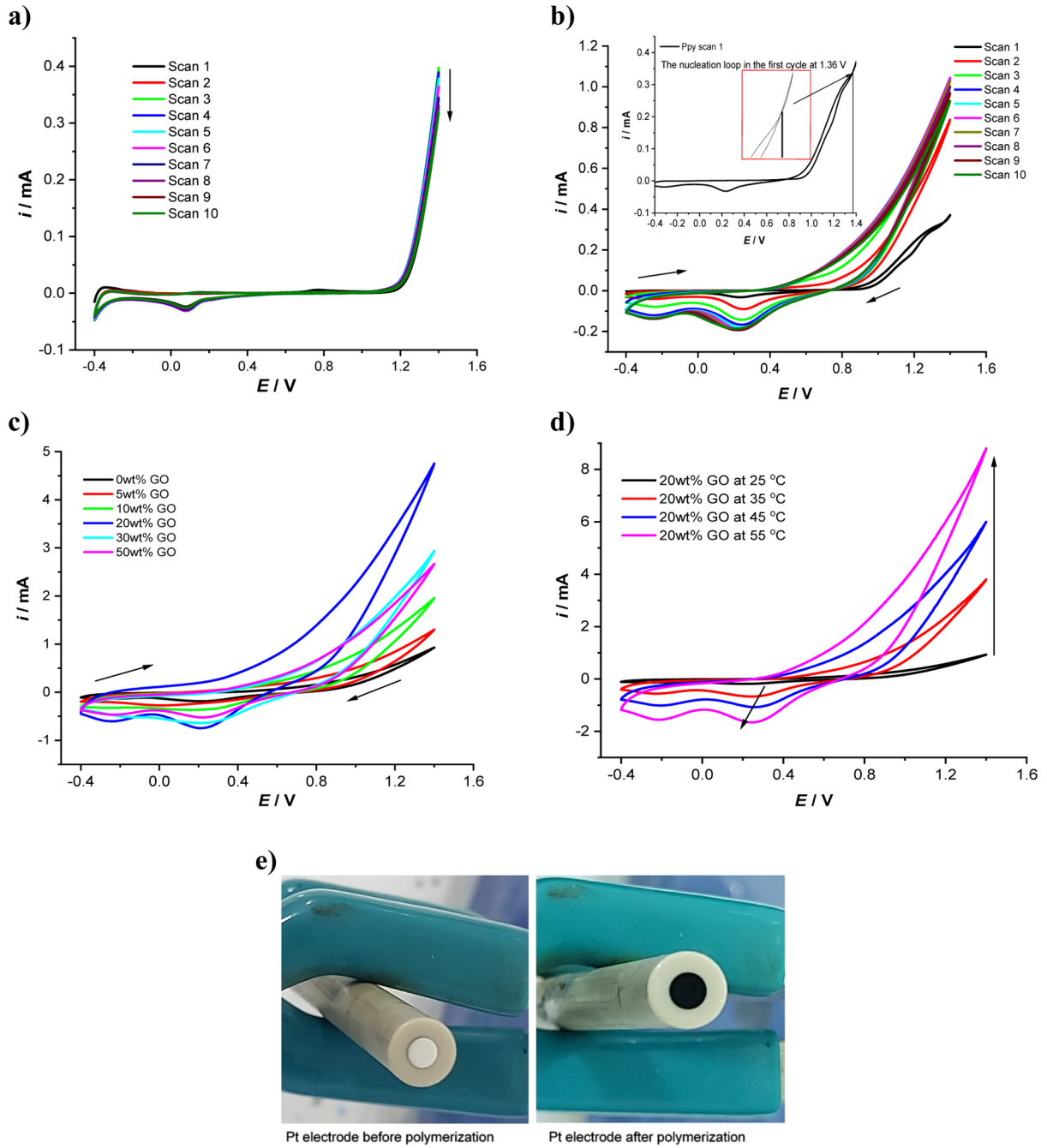

Figure 2. (a) CV of the blank electrolyte (1ChCl:2Phenol DES) on the WE electrode surface. CV of Ppy films deposited from 0.7 M pyrrole monomer in a 1ChCl:2Phenol DES at 25 °C, (b) 10 scans of the pure polymer (the inset shows the nucleation loop of Ppy film for scan 1), (c) different ratios of GO added, and (d) Ppy/GO (20 wt %) at various temperatures for deposition CV (b,c), with only scan 10 shown. The scan rate was 50 mV s^{-1}, and the potential range was between −0.4 and 1.4 V in all experiments. (e) Pt electrode before and after deposition of Ppy.

presented in our previous work.[41] The proposed structure and the details are shown in Figure S1.

2.4. Preparation of the Ppy and Ppy/GO-Modified Electrodes. The electropolymerization of the pyrrole monomer was performed via a CV method using a Pt working electrode (WE) with a 3 mm diameter, a Pt flag counter electrode with a surface area of 2 cm^2, and Ag wire (1 mm diameter) as a pseudo-reference electrode (RE). Ag/AgCl RE is not suitable for use in DESs as there is a liquid junction potential due to the difference between the viscosity of the electrolyte (Ag/AgCl) and DES solution, changing ion mobility. A silver wire was used as a pseudo-RE immersed into the DES solution, as reported in the literature;[13,42,43] for more details, see the Supporting Information, Section S2. Before depositing the thin-film polymer, the WE was polished using γ-alumina paste (0.05 μm), washed with deionized water, and dried. The polymer deposition was carried out in the DES (1ChCl:2Phenol) containing 0.7 M pyrrole monomer. The potential window was scanned from −0.4 to 1.4 V at a scan rate of 50 mV s^{-1} over 10 scans.

Ppy/GO composite polymer films were also synthesized in a similar manner to the formation of the Ppy films above, but with different weight ratios of GO present within the DES solution. The required quantity of GO was dispersed into the

https://doi.org/10.1021/acsomega.2c03882
ACS Omega XXXX, XXX, XXX−XXX

electrolyte (1ChCl:2Phenol) containing 0.7 M of pyrrole monomer and then ultrasonicated for 2 h to obtain a uniform dispersion. In this work, several samples of Ppy/GO were electrically polymerized in the DES (1ChCl:2Phenol) electrolyte with different masses of GO, that is, 5, 10, 20, 30, and 50 wt % of GO relative to pyrrole monomer.

After polymerization, the electrochemical stability of all deposited films was investigated via CV in an identical background electrolyte at temperatures of 25 and 50 °C. Other factors such as scan rate, scan number, and potential window were studied in this work—see the figure legends for each experiment.

2.5. Instruments. The electrochemical experiments were carried out via Interface 1010E GAMRY INSTRUMENTS (USA) in a cell system consisting of three electrodes, as discussed in Section 2.4. Electrochemical impedance spectroscopy (EIS) experiments for Ppy and Ppy/GO films were performed in the frequency range from 100,000 to 0.01 Hz with an amplitude of 10 mV, as recorded at +0.2 V at different temperatures. Further, the polymers synthesized in this study were characterized via the FTIR, XRD, SEM, and TEM techniques. The sample powders were dispersed in KBr pellets, and FTIR spectra were recorded in the range of 500−4000 cm^{-1} using a PerkinElmer Spectrum One FTIR spectrophotometer. Diffraction patterns of the polymer composites were examined using an X-ray spectrometer, model: PANalytical Empyrean, at 30 mA and 45 kV, and were scanned between 10 and 80° at 2θ. SEM images were recorded using a Phillips XL30 ESEM instrument, with an accelerator voltage of 15 keV. TEM images were recorded on a Philips CM 200 microscope at 200 kV.

3. RESULTS AND DISCUSSION

3.1. Electrochemical Characterization. *3.1.1. Electropolymerization of Ppy Films.* Figure 2a shows the CV of a blank electrolyte (1ChCl:2Phenol DES) at a scan rate of 50 mV s^{-1} without the pyrrole monomer, indicating no current response from the choline chloride/phenol mixtures on the WE electrode surface. Figure 2b shows the deposition CV for Ppy deposited on a Pt WE (3 mm dia.) in 1ChCl:2Phenol DES containing 0.7 M of pyrrole at a scan rate of 50 mV s^{-1} for 10 cycles and a potential range of −0.4 to 1.4 V. The CV shows both oxidation and reduction waves, characteristic of Ppy electrodeposition and growth, like that observed by Yavuz et al.[44−46] It is clear from Figure 2b that the growth of Ppy film increases with the increase of the scan number, demonstrated by an increase in the redox peaks. Inspection of the deposited electrode after polymerization shows the formation of a black solid polymer on the surface of WE, as shown in Figure 2e. This potential range was chosen for Ppy film electrodeposition as the oxidation of the monomer and nucleation of the polymer occur close to 1.4 V. In the first cycle, a nucleation loop was observed at 1.36 V, as shown in the inset in Figure 2b. It was observed that Ppy does not grow when the positive potential is less than 1.3 V. After the first scan, the nucleation loop vanished in the following cycles because of the persistent growth of the film, preventing further nucleation in subsequent scans. The specific capacitances (C_{sp}, F g^{-1}) of the samples of Ppy composite were determined using eq 1, where I is the current (A), Δt is the discharge time (s), ΔV is the potential change during discharge (V), and m is the mass of the active material of the electrode (g)[47]

$$C_{sp} = \frac{I \times \Delta t}{\Delta V \times m} \quad (1)$$

Figure 2c shows the 10th and final scan of the deposition CV where different quantities of GO were included in the deposition medium. Visual inspection of CV shows that all depositions where GO was present in the deposition medium have an increased cathodic and anodic wave compared to Ppy on its own; however, there is no general trend. In the presence of GO, the polymerization rate is increased for Ppy/GO films, but this was dependent on the composite electrode between pyrrole monomer in a weight ratio and GO, as shown in Figure 2c.

Generally, the rate of polymerization for Ppy/GO films was higher than that seen for pure Ppy due to more charge transfer onto the active sites of the electrodes enhancing Faradaic reaction in the Ppy/GO composite as a result of the increase in the surface area and active sites in the polymer composite. The specific capacitances of the Ppy/GO composites were calculated to be 167, 189, 197, 215, 190, and 175 F g^{-1}, respectively, for 0, 5, 10, 20, 30, and 50 wt % GO in the Ppy electrode. From these data, the specific capacitances for Ppy/GO films grown from 1ChCl:2Phenol DES relied on the microstructure of the Ppy/GO composite. The specific capacitance of Ppy/GO increases with increasing weight of the GO deposited up to 20 wt %. However, there is a subsequent decline in the specific capacitance when larger amounts of GO (30−50 wt %) were used in the Ppy samples. This discontinuity may be attributed to the higher ratio of GO particles, leading to agglomeration of GO on the surface of WE, reducing the surface area available for Ppy formation. As a result of GO agglomeration, diffusion of the monomer to the electrode surface becomes difficult, leading to a reduction in concentration of the monomer at the electrode surface, resulting in reduced polymer formation. Similar findings have been reported in the literature.[3] From the discussion above, it can be concluded that the highest specific capacitance is gained for 20 wt % GO mixed with Ppy, suggesting a synergistic effect between materials in this composite. Accordingly, Ppy films deposited from an electrolyte of 20 wt % GO were selected as the WE for the subsequent experiments.

In order to optimize the electrochemical performance of Ppy/GO, the influence of temperature change (25−55 °C) on the formation of films prepared from Ppy/GO(20 wt %) in 1ChCl:2Phenol was investigated at a scan rate 50 mV s^{-1}, as shown in Figure 2d (here, only scan 10 is shown for deposition CV), and its behavior was compared with that of the film prepared at 25 °C. The shapes of the associated cyclic voltammograms are similar to that described above. However, the films deposited at 55 °C demonstrated higher current responses and larger cathodic peak areas. This led to a greater specific capacitance than polymers grown at room temperature. Additionally, as the temperature increased, the anodic peaks for polymer growth shifted toward a more positive potential, and the peak current increased. As a result, a quantitatively larger deposition of the polymer on the surface occurred. The viscosity of the electrolyte (see Figure S2, viscosity measurements of 1ChCl:2Phenol DES with/without the monomer) decreases with increasing temperature, from 93.33 cP at 25 °C to 23.98 cP at 55 °C; as a result, there is acceleration of the diffusion of electroactive species, and it may be a significant contributor to these observations along with improved reaction kinetics at elevated temperatures.[48]

https://doi.org/10.1021/acsomega.2c03882
ACS Omega XXXX, XXX, XXX−XXX

The thickness of the polymers can be determined based on the amount of charge (Q) in the coulomb (C) under the cathodic peaks from the integral of the cathodic current with time for the last scan of the deposited film. The thicknesses (d) of all deposited polymers are reported in Table 1 and were estimated according to eq 2

$$d = \frac{QM}{2F\rho} \quad (2)$$

where Q is the amount of charge for the electrodeposition film (see Table 1), M is the molar mass of monomer (in g/mol), ρ is the polymer density (1.5 g cm^{-3}), and F is the Faraday constant (96,485 C mol^{-1}).

Table 1. Thicknesses and Charges of Ppy Films Deposited from Different Quantities of GO and Temperatures under Otherwise Identical Conditions, as per Figure 2

samples	temperature °C	Q/C of cathodic current 10th cycle	thickness (nm)
Ppy	25	0.00476	11.10
Ppy/GO (5 wt %)	25	0.00792	18.40
Ppy/GO (10 wt %)	25	0.01028	23.80
Ppy/GO (20 wt %)	25	0.02257	52.40
Ppy/GO (30 wt %)	25	0.01576	36.53
Ppy/GO (50 wt %)	25	0.01579	36.60
Ppy/GO (20 wt %)	35	0.02204	51.10
Ppy/GO (20 wt %)	45	0.03006	69.70
Ppy/GO (20 wt %)	55	0.05301	122.90

3.1.2. Effect of Potential Window on Electrochemical Performance of Ppy/GO Electrodeposited Films. In Section 3.1.1, comparisons were made between depositions at different temperatures and for different GO ratios in the polymer matrix. Here, we compare the behavior of the Ppy-modified electrode prepared from an electrolyte containing 0.7 M PPy with 20 wt % GO at 55 °C in a monomer-free 1ChCl:2Phenol DES for two potential windows. This was intended to distinguish the electrochemical response of the polymer composite in the electrolyte (monomer-free) and provide an indicator of a suitable potential range for charge/discharge. Figure 3a shows a cyclic voltammogram scanned from −0.4 to 1.4 V at a scan rate of 50 mV s^{-1} for 20 scans. At this potential range, poor stability was observed during the redox cycle with a reduction in both cathodic and anodic processes. Figure 3b shows an identical experiment, where a freshly deposited PPy/Gy polymer was cycled for a shorter potential range, from −0.4 to 0.8 V, to overcome the degradation of the polymer due to over-oxidation of the film at the extended potentials employed. The lower anodic potential of 0.8 V increases redox stability of the polymer. Interestingly, increased electrochemical activity was observed with increasing scan number. The data suggest that the formation of Ppy from 1ChCl:2Phenol DES containing 20 wt % GO allows for electrochemical stability in the supercapacitor within this potential window range. The long-term electrochemical stability of pure Ppy and Ppy/GO in DES was also studied, the results of which are presented and discussed in Section 3.1.4.

3.1.3. Comparison of Ppy and Ppy/GO Films at 25 and 55 °C. Film capacitance is an important factor in evaluating a pseudocapacitor performance. Figure 4 shows CV for Ppy and Ppy/GO films at 25 and 55 °C at varying scan rates. Ppy and Ppy/GO (20% wt) were prepared at 55 °C from 1ChCl-2Phenol DES under similar electropolymerization conditions (scan rate and potential windows), as described in Figure 2b for the pure polymer and Figure 2d for Ppy/GO(20% wt), but the deposition of the polymer was carried out over seven cycles for both polymers to reduce the thickness of deposited polymer. The calculated masses of the active electrodes were around 9.33 and 26.7 μg for pure Ppy and Ppy/GO (wt 20%), respectively, calculated from the reduction peak of the last scan of the deposited film. After the films were deposited on the Pt electrode, they were separately exposed to 1ChCl:2Phenol DES (monomer-free) at different temperatures and scan rates (5, 10, 20, 30, 40 50, and 100 mV s^{-1}) employing CV, where

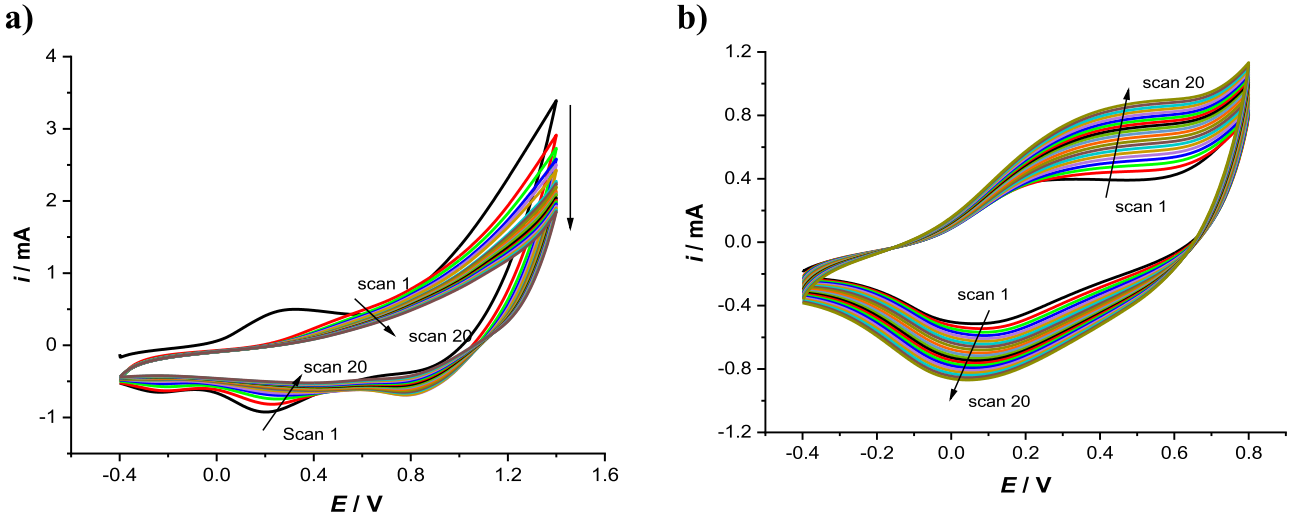

Figure 3. Effect of potential windows on the electrochemical performance of Ppy/GO (20 wt %) cycled in 1ChCl-2Phenol DES monomer-free electrolyte scanned from (a) −0.4 to 1.4 and (b) −0.4 to 0.8 V, with both at a scan rate of 50 mV s^{-1} and at 50 °C.

https://doi.org/10.1021/acsomega.2c03882
ACS Omega XXXX, XXX, XXX−XXX

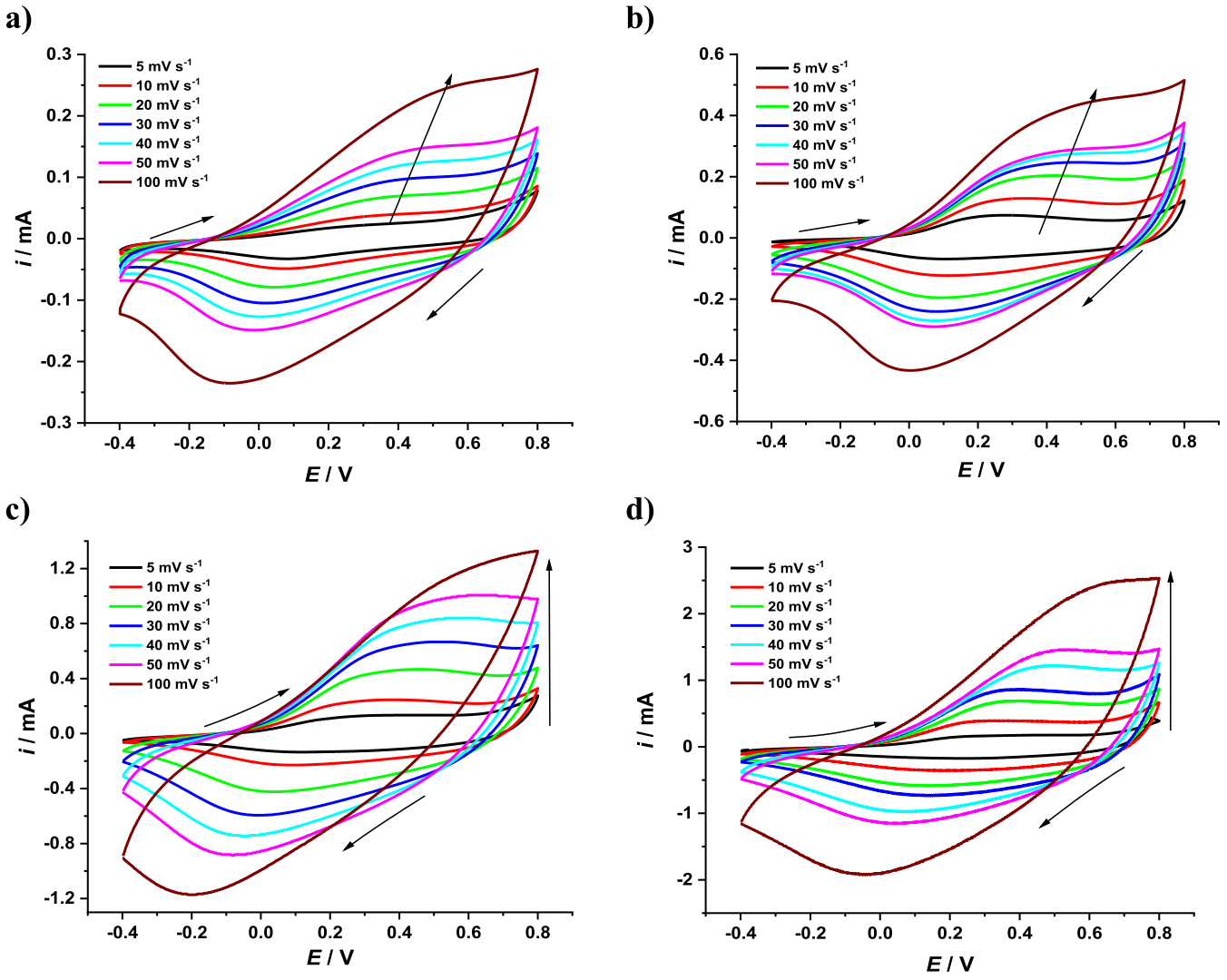

Figure 4. Cyclic voltammograms of polymers at different scan rates and temperatures. (a,b) Cyclic voltammograms of Ppy exposed to 1ChCl:2Phenol DES at 25 and 50 °C, respectively; (c,d) Cyclic voltammograms of Ppy/GO(20 wt %) exposed to 1ChCl:2Phenol DES at 25 and 50 °C, respectively.

Table 2. Specific Capacitances of Ppy and Ppy/GO Nanocomposites at Different Temperatures and Scan Rates

	specific capacitance (F g^{-1}) at various scan rates						
samples cycled in 1ChCl:2Phenol DSE electrolyte	5 mV s^{-1}	10 mV s^{-1}	20 mV s^{-1}	30 mV s^{-1}	40 mV s^{-1}	50 mV s^{-1}	100 mV s^{-1}
Ppy at 25 °C	341.46	261.66	217.53	194.67	177.70	166.20	124.26
Ppy/GO (20 wt %) at 25 °C	594.79	501.17	448.28	409.73	371.69	339.76	174.92
Ppy at 50 °C	853.34	744.02	572.75	457.14	376.53	317.19	226.87
Ppy/GO (20 wt %) at 50 °C	1071.78	821.63	655.24	546.04	525.55	485.08	353.21

the potential windows ranged from −0.4 to 0.8 V in all experiments. The cyclic voltammograms of pure Ppy and the Ppy/GO composite are shown in Figure 4. In each case, the current peaks increase with increasing scan rate, maintaining redox reactions (the shapes of cyclic voltammograms are quasi-rectangular) of all polymers, even at the highest scan rate (100 mV s^{-1}), but without which deviations in the peak current potential can be observed. This can be attributed to Faradaic capacitive behavior and double-layer capacitance in the polymer electrodes. The oxidation peaks shift toward a positive potential, while reduction peaks shift toward a negative potential with increasing scan rate. This is likely due to the enhanced resistance of the WE driving hysteresis due to the need for movement of counter-balancing ions moving in/out of the film.[3,49] Interestingly, hysteresis was reduced in both examples where GO was present in the deposition medium, despite increased quantities of PPy present and an increased magnitude of charge/discharge. One possibility may be the increased surface area of Ppy deposits formed due to growth on GO sheets in addition to the Pt WE surface, enabling diffusion in/out of the films at an increased rate. SEM observations in Section 3.2.1 are consistent with this proposal.

The change in specific capacitance versus scan rate for Ppy and Ppy/GO composites at the two different temperatures are presented in Table 2. Generally, the specific capacitances decreased with increasing scan rate, in agreement with previous

https://doi.org/10.1021/acsomega.2c03882
ACS Omega XXXX, XXX, XXX−XXX

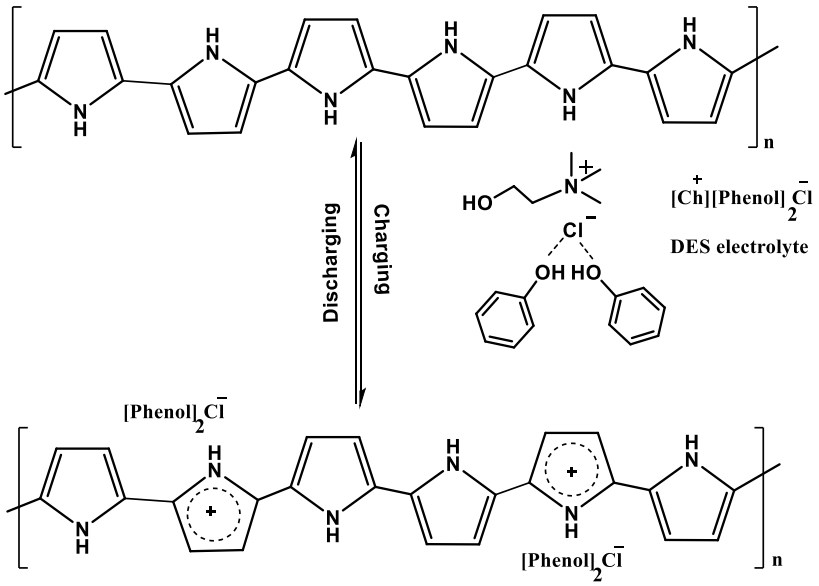

Figure 5. Schematic representation of the counteranion balancing the positive charges in the backbone of the polymer during oxidation at anodic potentials in a 1ChCl:2Phenol DES electrolyte.

Table 3. Comparison of the Specific Capacitances of the Ppy and Ppy/GO Supercapacitor Electrodes in Previous Work with Our Results (See Table 2) with Respect to Scan Rate

PPy composite electrode	electrolyte	scan rate mV s^{-1}	specific capacitance (F g^{-1})	references
PPy	in $EMIMBF_4$ IL $C_4(MIm)_2(BF_4)_2$	20	118, 222	55
PPy	ethaline−DES	50	1.9	45
PPy/graphene	1 M KCl solution	10	409	50
PPy/graphite	Reline−DES	10	446	44
multilayer synthesis of PPy/GO	1 M H_2SO_4	10	332	56
Ppy/graphene hydrogel	0.5 mol/L H_2SO_4	10	375	57
polypyrrole−CNT−graphene	sulfuric acid	5	453	58
Ppy and Ppy/GO	1ChCl:2Phenol at 25 °C	10	261.66 and 501.17	this work
Ppy and Ppy/GO	1ChCl:2Phenol at 50 °C	10	744.02 and 821.63	this work

works.[10,50] This can be related to the amount of charge per unit time, or in other words, there is not enough time for the ions to penetrate the surfaces of the polymers to allow the charge to be stored.[51] At high scan rates, fewer species are supplied from the bulk electrolyte to the deposited polymer film due to non-electrochemical equilibrium and limited diffusion rates during the switching processes. As a result, there is reduced charge storage and/or pseudocapacitance on the active electrode and the cyclic voltammogram shape tends to be more rectangular than quasi-rectangular.[52] The specific capacitances (calculated from the cyclic voltammograms in Figure 4 using eq 1) of the homopolymer (Ppy) in the electrolyte are lower than those for Ppy doped with 20 wt % GO at the same temperature (25 °C), the same electrolyte, and identical scan rates, as can be seen in Figure 4a,c. For example, the specific capacitance of Ppy was found to be 341.46 F g^{-1} at a 5 mV s^{-1} scan rate, while it increases to 594.79 F g^{-1} for Ppy doped with 20 wt % GO at the same scan rate and temperature. This is due to the GO particles increasing the porosity and surface area of the electrolytically active surface and thus decreasing its resistance to charge transfer. As a consequence, the reaction for the Ppy/GO film was diffusion-controlled, hence signifying ideal capacitive behavior.

The influence of the solution temperature on the specific capacitance for the same films that were exposed to 1ChCl:2Phenol DES electrolyte at 25 °C was also determined at 50 °C as function of scan rate. Similar behavior was found as the scan rate was increased, with the capacitive behavior reducing (Table 2) when the polymers were cycled at 50 °C, although the absolute specific capacitances were much higher than for the identical polymers at 25 °C. Here, we should explain a number of points: first, the effect of the solution temperature on cyclic voltammogram shape can be seen in Figure 4b,d with broader potential peaks and higher current peaks. Second, there is an increase in specific capacitance for both polymers in the 1ChCl:2Phenol DES electrolyte at 50 °C (i.e., Ppy and Ppy/GO composite), where the calculated C_{sp} at a constant scan rate of 5 mV s^{-1} for the Ppy/GO composite was 594.79 F g^{-1} and increased to 1071.78 F g^{-1} when the temperature of the electrolyte was changed from 25 °C (η = 90.12 cP) to 50 °C (η = 28.34 cP)—see Table 2 for more details. This is due to faster ion transfer between the electrode/electrolyte interfaces as the viscosity (η) of the solution decreases at the higher temperature (50 °C) compared to that at the lower temperature (25 °C), and the polymer becomes more porous; and therefore, the mobilities of species will increase.[53,54] EIS in Section 3.1.5 investigates this further.

The charge/discharge mechanism of electrodeposited Ppy films is anticipated to follow that of those deposited from aqueous media, where up to one pyrrole unit for every three within the polymer chain can hold positive charge, as stabilized through resonance with neighboring pyrrole units. The

https://doi.org/10.1021/acsomega.2c03882
ACS Omega XXXX, XXX, XXX−XXX

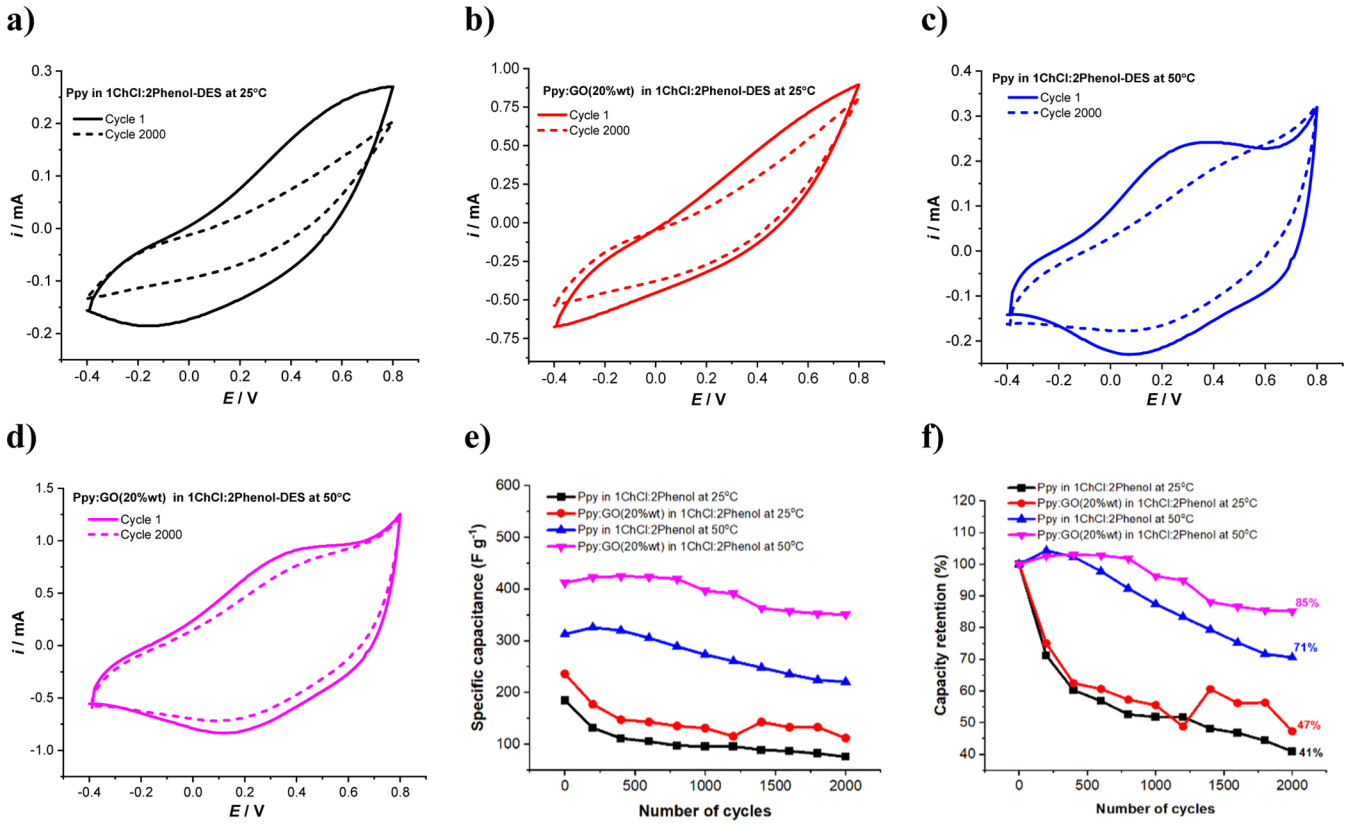

Figure 6. (a–d) CV curves and (e) cycling stability (specific capacitance) as a function of number of cycles for 2000 cycles for the Ppy and Ppy/GO (20% wt) composites at 50 mV s^{-1} and different temperatures in a 1ChCl:2Phenol DES electrolyte. (f) Capacity retention for 2000 cycles obtained from long-term electrochemical stability measurements of Ppy and Ppy/GO samples.

1ChCl:2Phenol DES formulation and coordination chemistry results in a complex anion $[Phenol]_2Cl^-$ in the choline chloride–phenol mixture, markedly different from those in aqueous solution, as described in the literature.[9,36] Therefore, the counteranion consisting of phenol and chloride can balance the positive charges in the backbone of the polymer during oxidation at anodic potentials during the oxidation of Ppys, as shown in Figure 5. Herein, our results showed good capacitances compared to other works in the recently published literature, as outlined in Table 3. From these data, we conclude that the Ppy/GO (20 wt %) composite has good reversibility behavior, possessing both pseudocapacitance and double-layer capacitance, with the capacitance higher than that of pure Ppy. Further, the capacitance and ion diffusion were increased at the higher temperature, even for the homopolymer (Ppy). Hence, the Ppy/GO composite in this study provides an exciting opportunity for reversible reactions and fast oxidation–reduction processes because Ppy/GO can be contributed to the pseudocapacitance of charge storage.

3.1.4. Cycling Stability. The cycling performance of Ppy composite electrodes provides an indication of the longevity of capacitive behavior for polymers that might be employed in supercapacitors. The long cycle life of the Ppy and Ppy/GO(20 wt %) electrodes was evaluated via CV techniques at a constant scan rate of 50 mV s^{-1} in 1ChCl:2Phenol DES at two different temperatures (25 and 50 °C) for 2000 cycles, as shown in Figure 6a-d (cycles 1 and 2000 are shown, while all 2000 cycles are presented in Figure S3). The potential window ranged from −0.4 to 0.8 V (versus Ag wire) in all experiments.

As depicted in Figure 6a,b, the CV of pure Ppy and Ppy/GO (20 wt %) in 1ChCl:2Phenol DES at 25 °C shows a quasi-rectangular shape, and the polymers progressively demonstrated a reduction in electroactivity during repeated charge and discharge processes. No redox peaks were present in either of the films after ∼200 cycles (see the Supporting Information, Figure S3), indicating that the rectangular behavior is more likely to be dominant. However, the increased temperature (50 °C) (Figure 6c,d) showed comparatively improved stability of the capacitive behavior for both the films without and with GO. The cyclic voltammograms were quasi-rectangular in form as well as displayed improved electrochemical performance. Further, the stable voltammograms demonstrate that there are redox peaks in the potential range for the Ppy and Ppy/GO (20 wt %) materials when the experiment is performed at the higher temperature (50 °C), suggesting that the present pseudocapacitive behavior (Faraday behavior) in Ppy and Ppy/GO films is dominant. This is likely due to the reduction in the solution viscosity when the temperature is increased and vice versa, enabling rapid supply of counter charge from the bulk electrolyte during electrochemical cycling. These results seem to be consistent with other research studies which found that capacitance and electrochemical stability are increased with decreasing viscosity due to the increase in temperature of the DES electrolyte.[48,59]

The calculated specific capacitance and capacitance retention as a function of cycle number for the Ppy and Ppy/GO (20 wt %) films at different temperatures are plotted in Figure 6e,f, respectively. At 25 °C, the specific capacitance of each of the materials [i.e., Ppy and Ppy/GO (20 wt %)]

https://doi.org/10.1021/acsomega.2c03882
ACS Omega XXXX, XXX, XXX−XXX

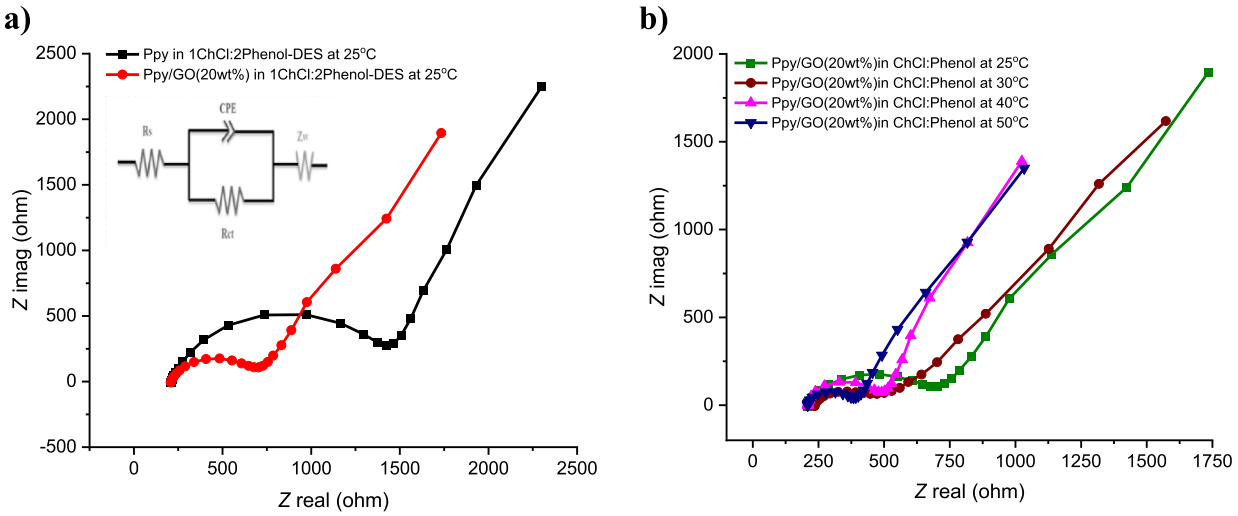

Figure 7. (a) Nyquist plot of Ppy films with/without GO (20 wt %) grown from 1ChCl:2Phenol DES at 55 °C and then exposed to the same background electrolyte at 25 °C. The inset represents the equivalent circuit of the polymer electrode. (b) Nyquist plots of Ppy/GO grown from 1ChCl:2Phenol DES and then exposed to 1ChCl:2Phenol DES electrolyte at various temperatures. In all experiments, the range of frequencies was 100 kHz to 0.01 Hz at an amplitude of 10 mV.

Table 4. Quantitative Results Obtained from Fitting the Data to the Equivalent Circuits Given in Figure 7

samples	electrolyte	temp. (°C)	R_s (Ω)	R_{ct} (Ω)	CPE (F)	Z_w (Ω)
Ppy	1ChCl:2Phenol	25	785	2038	2.7×10^{-6}	0.0001
Ppy/GO (20 wt %)	1ChCl:2Phenol	25	469	1306	1.3×10^{-5}	0.0007
Ppy/GO (20 wt %)	1ChCl:2Phenol	30	211	738	4.1×10^{-5}	0.0009
Ppy/GO (20 wt %)	1ChCl:2Phenol	40	53	249	9.5×10^{-5}	0.0085
Ppy/GO (20 wt %)	1ChCl:2Phenol	50	41	98	3.1×10^{-4}	0.007

decreases initially, although the capacitance of Ppy/GO (20 wt %) starts to increase at cycle 1400, remains stable until cycle 1800, and then decreases. At the higher temperature (i.e., at 50 °C), both the pure Ppy film and the Ppy/GO have an initial specific capacitance increase. For pure Ppy, it is increased by approximately 4% (325.64 F g^{-1}) from the original specific capacitance (312.33 F g^{-1}) and then reduced gradually over 2000 cycles, while for the Ppy/GO (20% wt) nanocomposite, the specific capacitance increases initially by up to 3% (424.48 F g^{-1}) from the initial capacitance (412.00 F g^{-1}) and then remains stable until cycle 800, after which it declines somewhat and then generally stays constant (~356 F g^{-1}) from cycle 1400 until the end of the experiment (cycle 2000).

Both temperature and the presence of GO in the Ppy film have a large effect on the cycling stability of the deposited films. The retention capacities of pure Ppy and Ppy/GO were 41 and 47%, respectively, at 25 °C. However, these two films had retention capacities of 71 and 85%, respectively, at 50 °C. Importantly, GO also improves stability to electrolytic cycling in addition to the increased deposition rates that were observed. Improvement in the electrochemical stability of the Ppy/GO (20 wt %) nanocomposite may relate to the synergistic effects between GO and Ppy, as confirmed by previous works,[3,60] where the former prevents damage to the structure of the polymer during the oxidation and reduction reactions. It can be concluded that the specific capacitance and cycling stability of Ppy films are greatly enhanced by the inclusion of GO compared to pure films. At room temperature (25 °C), the species mobility in 1ChCl:2Phenol DES is low, reducing the capacitive behavior of the films due to the high viscosity of the solution, restricting the segmental motion of the polymer chains at this temperature. However, at the higher temperature (i.e., 50 °C), the segmental motion of the polymer chain will increase, which makes the polymer more flexible. As a result, the mobility of the ions across the polymer/solution interface is also enhanced, therefore increasing the specific capacitance and cycling stability.

3.1.5. Impedance Study. Electrochemical impedance measurements were performed to investigate the electrochemical response that occurs at the polymer electrode/electrolyte interface that characterizes the electronic resistance, Faradaic pseudocapacitance, and double-layer capacitance of polymer electrodes. Ppy films with/without GO grown from 1ChCl:2Phenol DES were exposed to the same background electrolyte (monomer-free) under different temperatures. The results were extracted from Nyquist plots (the imaginary of the impedance vs the real) based on an equivalent circuit model illustrated in the inset of Figure 7a. Here, Nyquist data are fitted on R_s, CPE, R_{ct}, and Z_w, which are related to the solution resistance, constant-phase element, charge-transfer resistance, and Warburg impedance, respectively.

Generally, the semicircle is attributed to the charge-transfer reaction at the electrolyte/electrode interface (solution resistance, R_s), CPE represents the distributed capacitance of the interface/double layer of the film surface and the electrolyte, and the diameter of the curve gives an estimate of the charge-transfer resistance (R_{ct}), which indicates the rate at which charge can be transferred across the interface between the electrolyte and the film surface. The linear section in the low-frequency region is ascribed to Warburg impedance, which results from the ionic diffusion process in the electrode.[61,62] The charge-transfer resistance can be deduced from the

https://doi.org/10.1021/acsomega.2c03882
ACS Omega XXXX, XXX, XXX−XXX

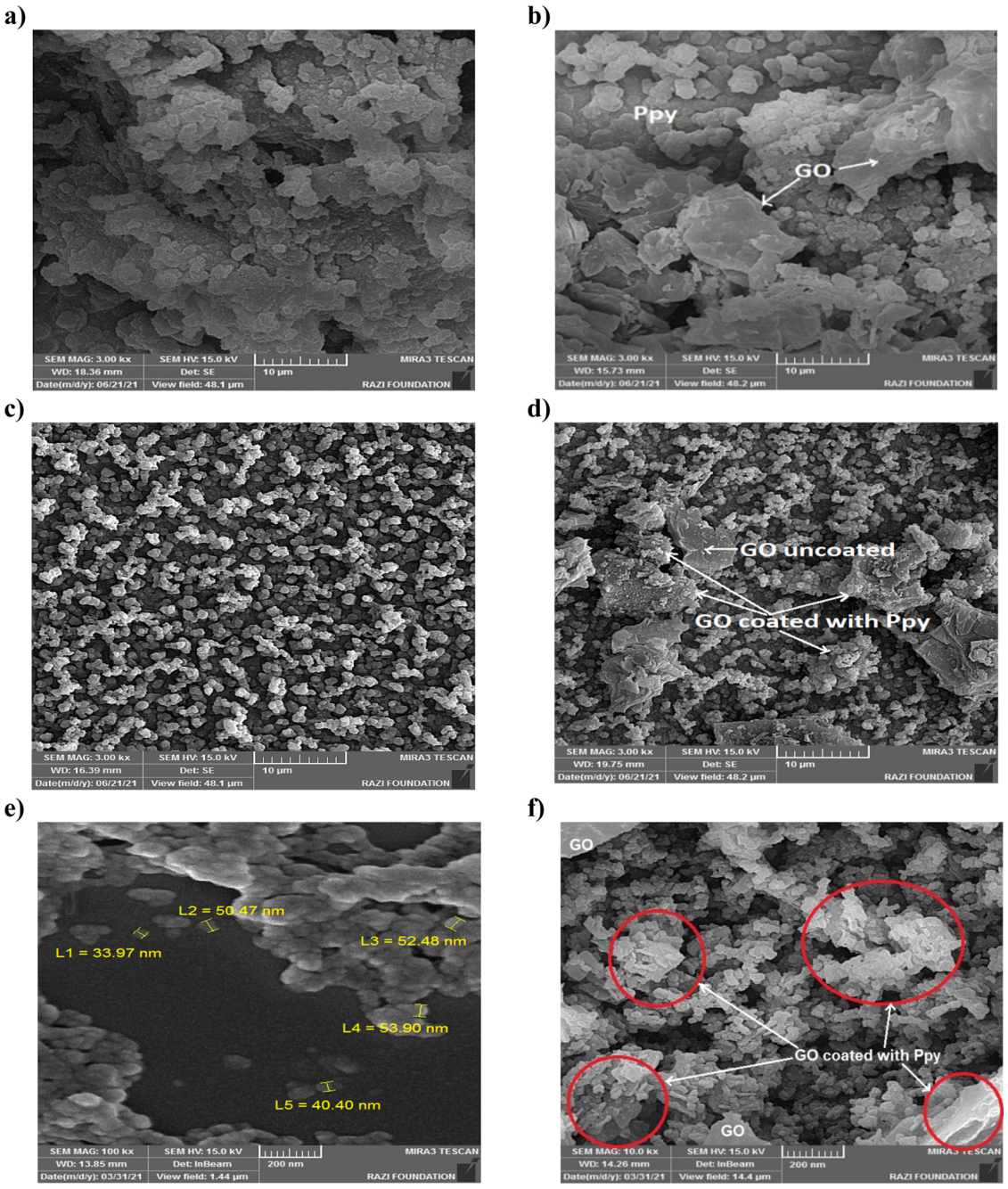

Figure 8. SEM images for (a) Ppy and (b) Ppy/20% GO grown from 1ChC:2Phenol DES at 25 °C and a potential window of −0.4 to 1.4 V for 7 scans at a scan rate of 50 mV s^{-1}, while images (c,d) show the same polymers under the same polymerization conditions but at 55 °C, respectively. Images (e,f) are magnifications of the SEM images for (c,d), respectively.

diameters of the semicircles. Here, a smaller diameter of the semicircle indicates a lower charge-transfer resistance and, consequently, a higher ionic conductivity. Measurements were recorded at a potential of +0.2 V. +0.2 V was selected after the deposited film was measured at different applied potentials in the same background electrolyte (monomer-free), as shown in Figure S4, with this potential showing the best Faradaic response and charge transfer at the polymer electrode/electrolyte interface. Figure 7a represents the EIS results of Ppy films with/without GO exposed to electrolytes (monomer-free) at 25 °C. In this figure, two Ppy films were separately grown from 1ChCl:2Phenol DES (similar to those produced in Section 3.1.3) exposed to 1ChCl:2Phenol (monomer-free) at 25 °C based on the background electrolyte of the deposited polymer.

As can be seen from Table 4, the highest resistance of the solution [R_s (Ω)] and the charge-transfer resistance (R_{ct}) were observed for the pure Ppy film (larger diameter) compared to Ppy/GO (smallest diameter), suggesting that the latter polymer has higher electrical conductivity and lower internal resistance and allows for fast transfer of species and electrons for redox supercapacitors, whereas the lower values for R_s and R_{ct} for the Ppy/GO film compared to the pure Ppy film are attributed to GO having a high charge-transfer resistance,[63] leading to a reduction to resistance to charge transfer compared to the pure film, facilitating the more effective

https://doi.org/10.1021/acsomega.2c03882
ACS Omega XXXX, XXX, XXX−XXX

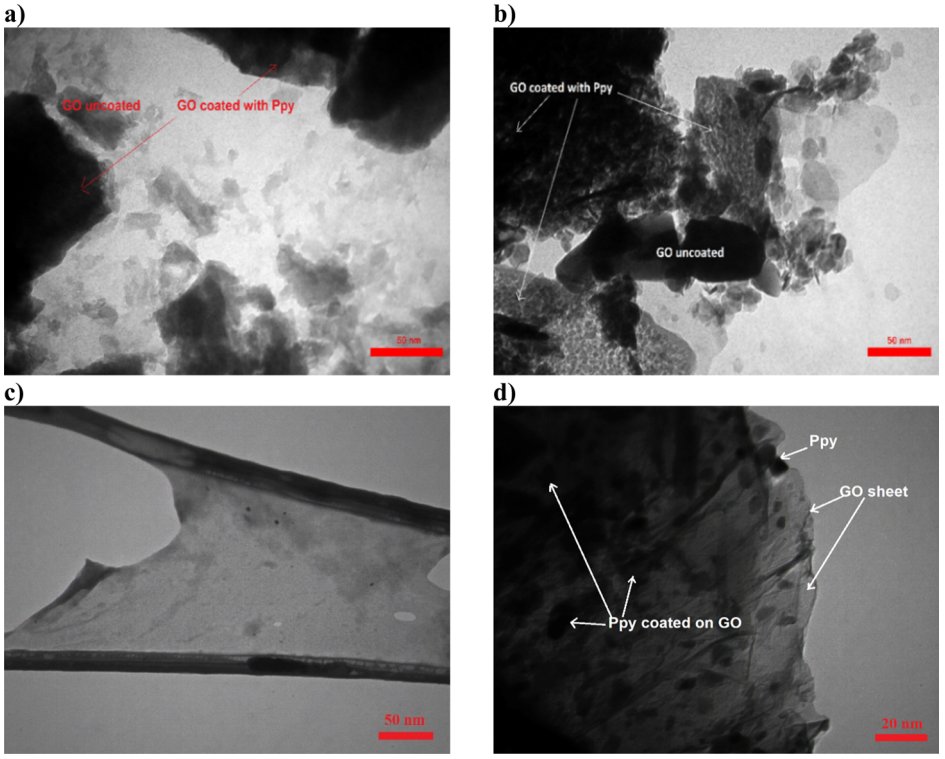

Figure 9. TEM images of Ppy/GO composite (a) at 25 °C and (b) at 50 °C produced by the electrochemical polymerization under similar conditions (a potential window of −0.4 to 1.4 V, a scan number of 7, a scan rate of 50 mV s^{-1}, and 0.7 M pyrrole) and (c) for pure GO, and (d) is the same sample (b) but at higher magnifications of the TEM image.

delivery of electrolyte ions to the surface of the polymer and with a shorter diffusion path.[64] In the case of Warburg impedance at the low-frequency part, the straight line indicates ion diffusion (Warburg impedance) in the bulk of the polymer electrode. It was found that a larger Warburg impedance was recorded for the Ppy/GO film compared to pure Ppy, suggesting that ion diffusion occurred more readily in the film grown from the DES containing GO compared to that without it.

Figure 7b represents the effects of temperature on Ppy/GO (as selected based on the above experiments) grown from 1ChCl:2Phenol DES and exposed to a 1ChCl:2Phenol electrolyte (monomer-free). Looking at the modeling data (Table 4), the resistance of the solution (R_s) and the charge-transfer resistance (R_{ct}) drastically decrease with increasing temperature, especially when the temperature of the electrolyte changes from 25 to 50 °C, indicating that the influence of temperature on R_s and R_{ct} is the most significant. Again, this is attributed to ion transfer for Ppy/GO film exposed to 1ChCl:2Phenol DES at 50 °C being much faster due to having the lowest viscosity and resistance, where R_{ct} is a significant kinetics factor that represents the charge-transfer process of the Faradaic reactions obtained on the polymer−electrolyte interfaces.[65] This means that the species diffuses faster in the polymer bulk at 50 °C than at 25 °C. This can be attributed to increased segmental motion of the polymer chain (more flexible) at a higher temperature. As a result, the mobility of ions in conducting polymer−electrolyte interfaces is faster. It was concluded that the smaller magnitudes of R_s and R_{ct} and an increase in the ionic conductivity (ions diffusion) are mainly favorable for supercapacitor applications for Ppy/GO composite grown from 1ChCl:2Phenol DES at 50 °C.

3.2. Structural Characterization. *3.2.1. Surface Morphology Study.* Figure 8 shows the investigation of the surface morphologies of Ppy films with/without GO (20 wt %) at two temperatures using SEM. The films were produced at 25 and 55 °C (other conditions are identical, such as a scan rate of 50 mV s^{-1}, a potential window of −0.4 to 1.4 V, a scan number of 7, and 0.7 M pyrrole) using CV.

Figure 8a depicts that the morphology of Ppy film at 25 °C has agglomerated as sub-micron sphere-like particles. Because of the agglomerated nature, there is a larger porous microstructure. The spherical particles persist in the Ppy film grown with 20 wt % GO at 25 °C (Figure 8b); however, sheets of GO can also be observed, which also contain some deposited Ppy on their surfaces. The surface morphologies of the Ppy films grown with/without GO at 55 °C are considerably different from those deposited at 25 °C. As shown in Figure 8c,d, the pure Ppy has a uniform surface with a porous sphere appearance, where the sizes of the particles are in the nanometer range of ∼50 nm (Figure 8e) and have a cauliflower appearance. Visual comparison with Figure 8a,b shows that these deposits have a much finer particle size. The smaller particle size may explain the observation that Ppy coatings deposited at 55 °C produced greater cyclability, likely due to the small size facilitating the mobility of species and electron transport during the oxidation and reduction reactions.[66] The surface structure of the Ppy films in Figure 8d is rather similar to those in Figure 8c when the GO (20 wt %) particles were added into the matrix, but the roughness and surface porosity of the film seem to be greater. The average grain size for the Ppy/GO film deposited at 55 °C is ∼70 nm, as shown in Figure 8f. The SEM image of pure GO is presented in Figure S1b in the Supporting Information. The TEM images of the Ppy/GO composite grown at 25 °C

https://doi.org/10.1021/acsomega.2c03882
ACS Omega XXXX, XXX, XXX−XXX

(Figure 9a) and 55 °C [Figure 9b,d (at higher magnification)] confirmed that the surface of the GO sheet is uniformly coated with Ppy and that the polymer is mainly absorbed onto the surface or intercalates with GO. Figure 9c provides a TEM image for pure GO sheets for comparison. Based on the observations, we conclude that the variation in the surface morphology of the polymers grown from a single electrolyte at different viscosities is consistent with the important variation in the electrochemical activities of these polymers, as found in the current work.

3.2.2. Fourier Transform Infrared Spectroscopy. FTIR spectra were used to elucidate the functional groups present in the samples (Ppy and Ppy composites). The FTIR spectra of Ppy and Ppy/GO and GO samples are shown in Figure 10.

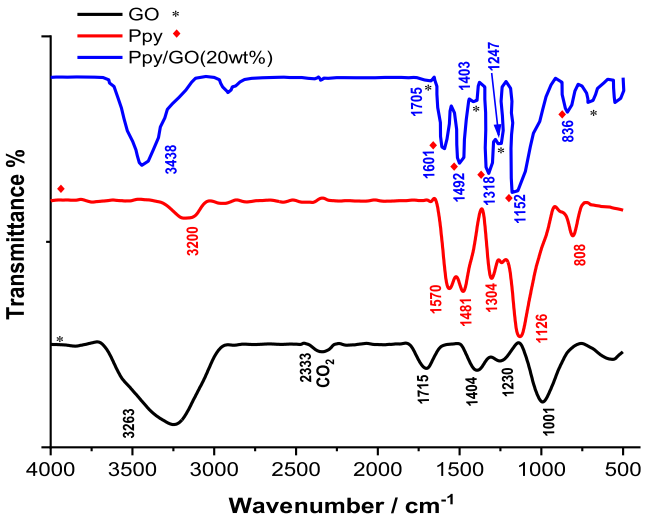

Figure 10. FTIR spectra of GO (black line), Ppy (red line), and Ppy/GO (blue line).

Herein, the interactions between the Ppy structure and functional groups on the surface of GO (−COOH, −OH, and epoxy groups) are affected through electrostatic, $\pi-\pi$, and hydrogen-bonding interactions. Initially, the electropolymerization of Ppy in a 1ChCl:2Phenol DES containing pyrrole at a concentration of 0.7 M was studied. The mechanism is likely to match that of aqueous systems, where pyrrole is oxidized at cathodic potentials, forming oxidized radicals that reductively eliminate $2H^+$ to form an α,α-pyrrole dimer. These dimers can then propagate to increased chain lengths through repeated oxidation and reaction with electrogenerated pyrrole radicals. The mechanism is shown in Figure S5.

For the GO sample, the broad absorption peak at 3264 cm^{-1} is attributed to an O−H stretching vibration, while the peak at 1715 cm^{-1} corresponds to a carbonyl (C═O) stretch. The other peaks in the GO layers are located at 1001, 1230, and 1404 cm^{-1}, which correspond to motions of the C−O of the epoxide group, C−O−C, and O−H deformation of the C−OH group, respectively.[67] In the FTIR spectrum of the Ppy ring, the absorption peaks observed at 3200, 1570, and 1481 cm^{-1} can be attributed to the N−H, C═C, and C−N stretching vibrations, respectively. In addition, other bands that could be ascribed to Ppy were observed at 1304, 1126, and 808 cm^{-1}, which can be ascribed to C−H in-plane stretching, C−N stretching, and the C−H out-of-plane bending vibrations of aromatic ring substitution in the polymers, respectively.[68]

In the case of the Ppy/GO composites, the strong broad peak at 3438 cm^{-1} is attributable to the O−H vibrations in GO along with the N−H stretching vibration that generally appears in the IR spectrum of Ppy. The band for the C═O group of GO appeared as a weak band that was downshifted to 1705 cm^{-1}. This could be due to $\pi-\pi$ interactions between the aromatic Ppy rings and GO layers. Other vibrations for functional groups of GO, such as the C−O−C and C−OH stretching vibrations, are apparent in the Ppy/GO composite and are shifted to 1247 and 1403 cm^{-1}, respectively. The epoxide group (C−O) of GO was not observed in the pure Ppy/GO sample, which can probably be attributed to being saturated by the adsorption peak of the Ppy ring. The band at 2919 cm^{-1} was assigned to asymmetric/symmetric vibrations of CH_2.[69] The peaks for C═C, C−N, C−H in-plane stretching, C−N stretching, and C−H out-of-plane stretching in the polymer composite were shifted to 1601, 1492, 1318, 1152, and 836 cm^{-1}, respectively, suggesting that Ppy/GO was successfully produced from the interaction between Ppy and GO due to the presence of functional groups, for instance, amine, carboxyl, epoxy, and hydroxyl groups.

3.2.3. X-ray Diffraction. The crystalline properties of the Ppy samples prepared via in situ polymerization (i.e., chemical polymerization using ammonium persulfate as an initiator; the detailed procedure is presented in the Supporting Information, Section S2) with/without 20 wt % of GO were investigated by XRD. The inset graph presented in Figure 11 shows a strong

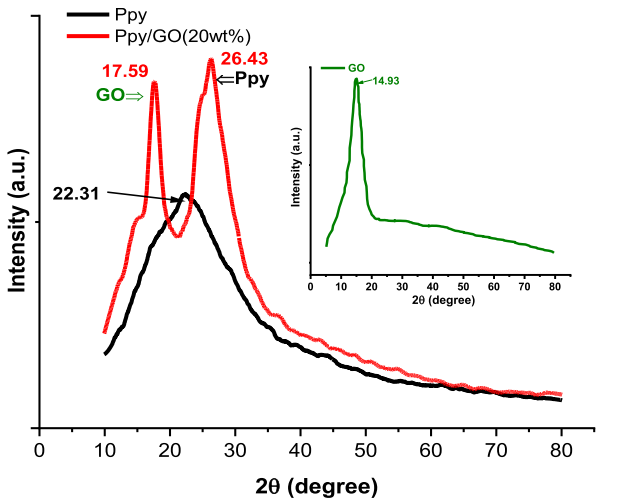

Figure 11. XRD patterns for GO (insert graph, green color), Ppy (black color), and Ppy/GO composite (red color) containing 20 wt % GO.

and sharp peak associated with GO at 14.92°, indicating the inclusion of the GO layer as sheets form within the deposit, which was also identified in earlier works.[70,71] For Ppy on its own, a characteristic peak is observed as a wide- and low-intensity diffraction peak at 2θ between 10 and 30°, with the maximum peak located at 22.1° that corresponds to the amorphous structure of Ppy. However, there are two sharp peaks in the Ppy/GO composite at 2θ, which are at 17.59 and 26.43° and can be attributed to GO sheets and the Ppy structure, respectively, that confirm the binding function between Ppy and GO. These results are similar to previous studies that have explored the relationships between Ppy and GO.[70] The high intensity and shifted absorption peaks of the

https://doi.org/10.1021/acsomega.2c03882
ACS Omega XXXX, XXX, XXX−XXX

composite indicate the increased polycrystalline behavior in the Ppy/GO composites compared to those of Ppy on its own. This, in addition to the evidence from SEM, TEM, and FTIR, suggests that there is a significant interaction between Ppy and GO in these electrodeposits.

4. CONCLUSIONS

In this paper, a DES of a 2:1 M ratio of phenol/choline chloride was used for the first time as an electrolyte for electrochemical polymerization of the pyrrole monomer with and without GO at different temperatures. It was observed that both the temperature and concentration of GO in the electrodeposition electrolyte play significant roles in determining both electrodeposition behavior and pseudocapacitance behavior. Polymers deposited at 55 °C had higher specific capacitances than those prepared at 25 °C. The presence of GO in the electrodeposition medium also increased specific capacitance; however, this reached a maximum at 20 wt % with respect to pyrrole concentration, and higher quantities of GO produced films with lower specific capacitance, likely due to agglomeration of GO at these increased concentrations. These observations were also extended to electrolytic cycling behavior and stability, where both elevated temperatures and the presence of GO in the electrodeposit resulted in significant increases in both specific capacitance and cycling stability. In the case of the Ppy/GO film cycled at 50 °C, this resulted in a specific capacitance of 1071.78 F g^{-1} at a scan rate of 5 mV s^{-1}, a value that outperforms other identified studies of Ppy composite electrodeposits. This film had a cycling stability of 85% over 2000 scans for the trials presented here, demonstrating a significant improvement over those prepared at a lower temperature and/or in the absence of GO. EIS confirmed the enhancement in the capacitances at high temperature was due to the increased mobility of ions in the electrolyte and decreased charge-transfer resistance.

The polymer materials were structurally characterized via FTIR, XRD, SEM, and TEM. FTIR and XRD demonstrate the production of Ppy and the presence of GO in the Ppy composite as well as a strong interaction between GO and Ppy. Regarding the surface morphologies, it was found that the morphologies of the films changed according to the temperature of the electrolyte used, where SEM and TEM measurements indicated that Ppy nanoparticles formed at a high temperature (55 °C). Further, the enhancement of the specific capacitance at 50 °C indicates the possibility of using the Ppy/GO compound as a supercapacitor electrode for high-temperature energy storage applications, for example, automobiles or similar applications in which the electrode is exposed to higher temperatures.

■ ASSOCIATED CONTENT

Supporting Information

The Supporting Information is available free of charge at https://pubs.acs.org/doi/10.1021/acsomega.2c03882.

Procedure for the synthesis of GO from graphite powder, along with the proposed structure of GO and SEM images; procedure for the chemical polymerization and formation of Ppy and PPy/GO powders used in XRD analysis; justification for the use of Ag wire RE and outline of the complexities in obtaining a suitable RE for DES media; measurements of viscosity of 1:2 ChCl/Phenol DES at varied temperatures without/with 0.7 M pyrrole; study of cycling stability of Ppy and Ppy/GO films at 25 and 50 °C; effect of electrical potential on electrochemical impedance measurements with Nyquist plots of Ppy/GO films at potentials from −0.2 to +0.6 V; proposed mechanisms for the electropolymerization of pyrrole from 1ChCl:2Phenol DES; and example calculations for generation of specific capacitance values from recorded data (PDF)

■ AUTHOR INFORMATION

Corresponding Authors

Hani K. Ismail − *Department of Chemistry, Faculty of Science and Health, Koya University, Koya KOY45 Kurdistan Region-F.R., Iraq*; orcid.org/0000-0001-5407-1806; Email: hani.khalil@koyauniversity.org

Jalil H. Kareem − *Petroleum Technology Department, Erbil Technology College, Erbil Polytechnic University, Erbil 44001 Kurdistan Region, Iraq*; Email: jalil.kareem@epu.edu.iq

Authors

Idrees B. Qader − *Pharmaceutical Chemistry Department, College of Pharmacy, Hawler Medical University, Erbil 44001 Kurdistan Region, Iraq*

Hasan F. Alesary − *Department of Chemistry, College of Science, University of Kerbala, Karbala 56001, Iraq*; orcid.org/0000-0002-3116-5145

Andrew D. Ballantyne − *Institute for Creative Leather Technologies, University of Northampton, Northampton NN1 5PH, U.K.*

Complete contact information is available at: https://pubs.acs.org/10.1021/acsomega.2c03882

Notes

The authors declare no competing financial interest.

■ ACKNOWLEDGMENTS

The authors would like to thank the Scientific Research Centre in EPU for their facilities and help. The authors would also like to thank Dr Mark Watkins from the University of Leicester for proofreading this manuscript.

■ REFERENCES

(1) Chandel, M.; Makkar, P.; Ghosh, N. N. Ag−Ni nanoparticle anchored reduced graphene oxide nanocomposite as advanced electrode material for supercapacitor application. *ACS Appl. Electron. Mater.* **2019**, *1*, 1215−1224.

(2) Alcaraz-Espinoza, J. J.; de Melo, C. P.; de Oliveira, H. P. Fabrication of highly flexible hierarchical polypyrrole/carbon nanotube on eggshell membranes for supercapacitors. *ACS Omega* **2017**, *2*, 2866−2877.

(3) Lim, Y.; Tan, Y.; Lim, H.; Huang, N.; Tan, W. Preparation and characterization of polypyrrole/graphene nanocomposite films and their electrochemical performance. *J. Polym. Res.* **2013**, *20*, 1−10.

(4) Das, A. K.; Paria, S.; Maitra, A.; Halder, L.; Bera, A.; Bera, R.; Si, S. K.; De, A.; Ojha, S.; Bera, S.; Karan, S. K.; Khatua, B. B. Highly rate capable nanoflower-like NiSe and WO_3@ PPy composite electrode materials toward high energy density flexible all-solid-state asymmetric supercapacitorr. *ACS Appl. Electron. Mater.* **2019**, *1*, 977−990.

(5) Fusalba, F.; Bélanger, D. Electropolymerization of polypyrrole and polyaniline− polypyrrole from organic acidic medium. *J. Phys. Chem. B* **1999**, *103*, 9044−9054.

(6) Cao, P.; Fan, Y.; Yu, J.; Wang, R.; Song, P.; Xiong, Y. Polypyrrole nanocomposites doped with functional ionic liquids for high performance supercapacitors. *New J. Chem.* **2018**, *42*, 3909−3916.

(7) Li, J.; Xie, H. Synthesis of graphene oxide/polypyrrole nanowire composites for supercapacitors. *Mater. Lett.* **2012**, *78*, 106−109.
(8) Jurewicz, K.; Delpeux, S.; Bertagna, V.; Beguin, F.; Frackowiak, E. Supercapacitors from nanotubes/polypyrrole composites. *Chem. Phys. Lett.* **2001**, *347*, 36−40.
(9) Ismail, H. K.; Alesary, H. F.; Juma, J. A.; Hillman, A. R.; Ryder, K. S. A comparative study of the formation, and ion and solvent transport of polyaniline in protic liquid-based deep eutectic solvents and aqueous solutions using EQCM. *Electrochim. Acta* **2022**, *418*, 140348.
(10) Abdah, M. A. A. M.; Razali, N. S. M.; Lim, P. T.; Kulandaivalu, S.; Sulaiman, Y. One-step potentiostatic electrodeposition of polypyrrole/graphene oxide/multi-walled carbon nanotubes ternary nanocomposite for supercapacitor. *Mater. Chem. Phys.* **2018**, *219*, 120−128.
(11) Almtiri, M.; Dowell, T. J.; Giri, H.; Wipf, D. O.; Scott, C. N. Electrochemically Stable Carbazole-Derived Polyaniline for Pseudocapacitors. *ACS Appl. Polym. Mater.* **2022**, *4*, 3088−3097.
(12) Weidlich, C.; Mangold, K.-M.; Jüttner, K. Conducting polymers as ion-exchangers for water purification. *Electrochim. Acta* **2001**, *47*, 741−745.
(13) Ismail, H. K.; Alesary, H. F.; Al-Murshedi, A. Y.; Kareem, J. H. Ion and solvent transfer of polyaniline films electrodeposited from deep eutectic solvents via EQCM. *J. Solid State Electrochem.* **2019**, *23*, 3107−3121.
(14) Pud, A. Stability and degradation of conducting polymers in electrochemical systems. *Synth. Met.* **1994**, *66*, 1−18.
(15) Lu, W.; Fadeev, A. G.; Qi, B.; Smela, E.; Mattes, B. R.; Ding, J.; Spinks, G. M.; Mazurkiewicz, J.; Zhou, D.; Wallace, G. G.; MacFarlane, D. R.; Forsyth, S. A.; Forsyth, M. Use of ionic liquids for π-conjugated polymer electrochemical devices. *Science* **2002**, *297*, 983−987.
(16) Pandey, K.; Yadav, P.; Mukhopadhyay, I. Elucidating different mass flow direction induced polyaniline−ionic liquid interface properties: insight gained from DC voltammetry and impedance spectroscopy. *J. Phys. Chem. B* **2014**, *118*, 3235−3242.
(17) Sekiguchi, K.; Atobe, M.; Fuchigami, T. Electropolymerization of pyrrole in 1-ethyl-3-methylimidazolium trifluoromethanesulfonate room temperature ionic liquid. *Electrochem. Commun.* **2002**, *4*, 881−885.
(18) Viau, L.; Hihn, J.; Lakard, S.; Moutarlier, V.; Flaud, V.; Lakard, B. Full characterization of polypyrrole thin films electrosynthesized in room temperature ionic liquids, water or acetonitrile. *Electrochim. Acta* **2014**, *137*, 298−310.
(19) Fernandes, P. M.; Campiña, J. M.; Pereira, N. M.; Pereira, C. M.; Silva, F. Biodegradable deep-eutectic mixtures as electrolytes for the electrochemical synthesis of conducting polymers. *J. Appl. Electrochem.* **2012**, *42*, 997−1003.
(20) Hansen, B. B.; Spittle, S.; Chen, B.; Poe, D.; Zhang, Y.; Klein, J. M.; Horton, A.; Adhikari, L.; Zelovich, T.; Doherty, B. W.; Gurkan, B.; Maginn, E. J.; Ragauskas, A.; Dadmun, M.; Zawodzinski, T. A.; Baker, G. A.; Tuckerman, M. E.; Savinell, R. F.; Sangoro, J. R. Deep eutectic solvents: A review of fundamentals and applications. *Chem. Rev.* **2020**, *121*, 1232−1285.
(21) Abbott, A. P.; Capper, G.; Davies, D. L.; Rasheed, R. K.; Tambyrajah, V. Novel solvent properties of choline chloride/urea mixtures. *Chem. Commun.* **2003**, *10*, 70−71.
(22) Alesary, H. F.; Ismail, H. K.; Odda, A. H.; Watkins, M. J.; Majhool, A. A.; Ballantyne, A. D.; Ryder, K. S. Influence of different concentrations of nicotinic acid on the electrochemical fabrication of copper film from an ionic liquid based on the complexation of choline chloride-ethylene glycol. *J. Electroanal. Chem.* **2021**, *897*, 115581.
(23) Tomé, L. I.; Baião, V.; da Silva, W.; Brett, C. M. Deep eutectic solvents for the production and application of new materials. *Appl. Mater. Today* **2018**, *10*, 30−50.
(24) Ismail, H. K. Electrodeposition of a mirror zinc coating from a choline chloride-ethylene glycol-based deep eutectic solvent modified with methyl nicotinate. *J. Electroanal. Chem.* **2020**, *876*, 114737.
(25) Alesary, H. F.; Ismail, H. K.; Shiltagh, N. M.; Alattar, R. A.; Ahmed, L. M.; Watkins, M. J.; Ryder, K. S. Effects of additives on the electrodeposition of ZnSn alloys from choline chloride/ethylene glycol-based deep eutectic solvent. *J. Electroanal. Chem.* **2020**, *874*, 114517.
(26) Alabdullah, S. S.; Ismail, H. K.; Ryder, K. S.; Abbott, A. P. Evidence supporting an emulsion polymerisation mechanism for the formation of polyaniline. *Electrochim. Acta* **2020**, *354*, 136737.
(27) Ismail, H. K. *Novel battery chemistries using electrically conducting polymers synthesised from deep eutectic solvents and aqueous solutions*; University of Leicester, 2017.
(28) Kareem, J. H.; Abbott, A. P.; Ryder, K. Shifting desulfurization equilibria in ionic liquid−oil mixtures. *Energy Fuel.* **2019**, *33*, 1106−1113.
(29) Abbott, A. P.; Ahmed, E. I.; Prasad, K.; Qader, I. B.; Ryder, K. S. Liquid pharmaceuticals formulation by eutectic formation. *Fluid Phase Equilib.* **2017**, *448*, 2−8.
(30) Qu, W.; Qader, I. B.; Abbott, A. P. Controlled release of pharmaceutical agents using eutectic modified gelatin. *Drug Delivery Transl. Res.* **2021**, *12*, 1187.
(31) Smith, E. L.; Abbott, A. P.; Ryder, K. S. Deep eutectic solvents (DESs) and their applications. *Chem. Rev.* **2014**, *114*, 11060−11082.
(32) Zhang, Q.; Vigier, K. D. O.; Royer, S.; Jérôme, F. Deep eutectic solvents: syntheses, properties and applications. *Chem. Soc. Rev.* **2012**, *41*, 7108−7146.
(33) Alesary, H. F.; Khudhair, A. F.; Rfaish, S. Y.; Ismail, H. K. Effect of sodium bromide on the electrodeposition of Sn, Cu, Ag and Ni from a deep eutectic solvent-based ionic liquid. *Int. J. Electrochem. Sci.* **2019**, *14*, 7116−7132.
(34) Ismail, H. K.; Alesary, H. F.; Mohammed, M. Q. Synthesis and characterisation of polyaniline and/or MoO_2/graphite composites from deep eutectic solvents via chemical polymerisation. *J. Polym. Res.* **2019**, *26*, 65.
(35) Hillman, A. R.; Ryder, K. S.; Ismail, H. K.; Unal, A.; Voorhaar, A. Fundamental aspects of electrochemically controlled wetting of nanoscale composite materials. *Faraday Discuss.* **2017**, *199*, 75−99.
(36) Hillman, A. R.; Ryder, K. S.; Ferreira, V. C.; Zaleski, C. J.; Vieil, E. Ion transfer dynamics of poly (3, 4-ethylenedioxythiophene) films in deep eutectic solvents. *Electrochim. Acta* **2013**, *110*, 418−427.
(37) Kaynak, A. Effect of synthesis parameters on the surface morphology of conducting polypyrrole films. *Mater. Res. Bull.* **1997**, *32*, 271−285.
(38) Alesary, H. F.; Ismail, H. K.; Mohammed, M. Q.; Mohammed, H. N.; Abbas, Z. K.; Barton, S. A comparative study of the effect of organic dopant ions on the electrochemical and chemical synthesis of the conducting polymers polyaniline, poly (o-toluidine) and poly (o-methoxyaniline). *Chem. Pap.* **2021**, *75*, 5087−5101.
(39) Nguyen, P. T.; Nguyen, T. D. T.; Nguyen, V. S.; Dang, D. T. X.; Le, H. M.; Wei, T. C.; Tran, P. H. Application of deep eutectic solvent from phenol and choline chloride in electrolyte to improve stability performance in dye-sensitized solar cells. *J. Mol. Liq.* **2019**, *277*, 157−162.
(40) Qader, I. B.; Kareem, J. H.; Ismail, H. K.; Mahmood, H. K. Novel phenolic deep eutectic solvents for desulfurisation of petrodiesel. *Karbala Int. J. Mod. Sci.* **2021**, *7*, 12.
(41) Ismail, H. K.; Ali, L. I. A.; Alesary, H. F.; Nile, B. K.; Barton, S. Synthesis of a poly (p-aminophenol)/starch/graphene oxide ternary nanocomposite for removal of methylene blue dye from aqueous solution. *J. Polym. Res.* **2022**, *29*, 1−22.
(42) Erdogan, P. Y.; Zengin, H.; Yavuz, A. Growth and cycling of polyaniline electrode in a deep eutectic solvent: A new electrolyte for supercapacitor applications. *Solid State Ionics* **2020**, *352*, 115362.
(43) Shen, X.; Sinclair, N.; Wainright, J.; Akolkar, R.; Savinell, R. Evaluating and Developing a Reliable Reference Electrode for Choline Chloride Based Deep Eutectic Solvents. *J. Electrochem. Soc.* **2020**, *167*, 086509.
(44) Ozdemir, N.; Zengin, H.; Yavuz, A. Electropolymerization of pyrrole from a deep eutectic solvent for supercapacitor applications. *Mater. Chem. Phys.* **2020**, *256*, 123645.

https://doi.org/10.1021/acsomega.2c03882
ACS Omega XXXX, XXX, XXX−XXX

(45) Yavuz, A.; Aktaş, S.; Durdu, S. Polypyrrole Modified Graphite Electrode for Supercapacitor Application: The Effect of Cycling Electrolytes. *J. Sci.* **2019**, *23*, 462−471.
(46) Yavuz, A.; Ozdemir, N.; Zengin, H. Polypyrrole-coated tape electrode for flexible supercapacitor applications. *Int. J. Hydrogen Energy* **2020**, *45*, 18876−18887.
(47) Pal, K.; Panwar, V.; Bag, S.; Manuel, J.; Ahn, J. H.; Kim, J. K. Graphene oxide−polyaniline−polypyrrole nanocomposite for a supercapacitor electrode. *RSC Adv.* **2015**, *5*, 3005−3010.
(48) Zhong, M.; Tang, Q. F.; Zhu, Y. W.; Chen, X. Y.; Zhang, Z. J. An alternative electrolyte of deep eutectic solvent by choline chloride and ethylene glycol for wide temperature range supercapacitors. *J. Power Sources* **2020**, *452*, 227847.
(49) Yan, J.; Wei, T.; Shao, B.; Fan, Z.; Qian, W.; Zhang, M.; Wei, F. Preparation of a graphene nanosheet/polyaniline composite with high specific capacitance. *Carbon* **2010**, *48*, 487−493.
(50) Sahoo, S.; Karthikeyan, G.; Nayak, G. C.; Das, C. K. Electrochemical characterization of in situ polypyrrole coated graphene nanocomposites. *Synth. Met.* **2011**, *161*, 1713−1719.
(51) Zhang, D.; Dong, Q.-Q.; Wang, X.; Yan, W.; Deng, W.; Shi, L.-Y. Preparation of a three-dimensional ordered macroporous carbon nanotube/polypyrrole composite for supercapacitors and diffusion modeling. *J. Phys. Chem. C* **2013**, *117*, 20446−20455.
(52) Wang, K.; Huang, J.; Wei, Z. Conducting polyaniline nanowire arrays for high performance supercapacitors. *J. Phys. Chem. C* **2010**, *114*, 8062−8067.
(53) Li, W.; Xu, K.; An, L.; Jiang, F.; Zhou, X.; Yang, J.; Chen, Z.; Zou, R.; Hu, J. Effect of temperature on the performance of ultrafine MnO 2 nanobelt supercapacitors. *J. Mater. Chem. A* **2014**, *2*, 1443−1447.
(54) Dar, F. I.; Moonoosawmy, K. R.; Es-Souni, M. Morphology and property control of NiO nanostructures for supercapacitor applications. *Nanoscale Res. Lett.* **2013**, *8*, 363.
(55) Lee, W. G.; Cho, W. J.; Whang, Y. H.; Raj, C. J.; Kim, B. C.; Park, J. H.; Yu, K. H. Feasible study of polypyrrole film in single and double cationic ionic liquids as novel electrolytes for energy storage applications. *Synth. Met.* **2016**, *222*, 274−284.
(56) Salas, I. M. D. l. F.; Sudhakar, Y.; Selvakumar, M. High performance of symmetrical supercapacitor based on multilayer films of graphene oxide/polypyrrole electrodes. *Appl. Sur. Sci.* **2014**, *296*, 195−203.
(57) Zhang, F.; Xiao, F.; Dong, Z. H.; Shi, W. Synthesis of polypyrrole wrapped graphene hydrogels composites as supercapacitor electrodes. *Electrochim. Acta* **2013**, *114*, 125−132.
(58) Aphale, A.; Maisuria, K.; Mahapatra, M. K.; Santiago, A.; Singh, P.; Patra, P. Hybrid electrodes by in-situ integration of graphene and carbon-nanotubes in polypyrrole for supercapacitors. *Sci. Rep.* **2015**, *5*, 1−8.
(59) Yang, H.; Sang, M.; Li, G.; Zuo, D.; Xu, J.; Zhang, H. Stretchable, self-healable, conductive and adhesive gel polymer electrolytes based on a deep eutectic solvent for all-climate flexible electrical double-layer capacitors. *J. Energy Storage* **2022**, *45*, 103766.
(60) Ghanbari, R.; Shabestari, M. E.; Kalali, E. N.; Hu, Y.; Ghorbani, S. R. Electrochemical performance and complex impedance properties of reduced-graphene oxide/polypyrrole nanofiber nanocomposite. *Ionics* **2021**, *27*, 1279−1290.
(61) Liao, L.; Zuo, P.; Ma, Y.; Chen, X.; An, Y.; Gao, Y.; Yin, G. Effects of temperature on charge/discharge behaviors of LiFePO4 cathode for Li-ion batteries. *Electrochim. Acta* **2012**, *60*, 269−273.
(62) Ding, C.; Nohira, T.; Fukunaga, A.; Hagiwara, R. Charge-discharge performance of an ionic liquid-based sodium secondary battery in a wide temperature range. *Electrochemistry* **2015**, *83*, 91−94.
(63) Casero, E.; Parra-Alfambra, A.; Petit-Domínguez, M.; Pariente, F.; Lorenzo, E.; Alonso, C. Differentiation between graphene oxide and reduced graphene by electrochemical impedance spectroscopy (EIS). *Electrochem. Commun.* **2012**, *20*, 63−66.
(64) Stoller, M. D.; Park, S.; Zhu, Y.; An, J.; Ruoff, R. S. Graphene-based ultracapacitors. *Nano Lett.* **2008**, *8*, 3498−3502.
(65) Yang, S.; Song, H.; Chen, X. Electrochemical performance of expanded mesocarbon microbeads as anode material for lithium-ion batteries. *Electrochem. Commun.* **2006**, *8*, 137−142.
(66) Lv, P.; Meng, Y.; Song, L.; Pang, H.; Liu, W. A self-supported electrode for supercapacitors based on nanocellulose/multi-walled carbon nanotubes/polypyrrole composite. *RSC Adv.* **2021**, *11*, 1109−1114.
(67) McAllister, M. J.; Li, J.-L.; Adamson, D. H.; Schniepp, H. C.; Abdala, A. A.; Liu, J.; Herrera-Alonso, M.; Milius, D. L.; Car, R.; Prud'homme, R. K. Single sheet functionalized graphene by oxidation and thermal expansion of graphite. *Chem. Mater.* **2007**, *19*, 4396−4404.
(68) Zhou, H.; Zhang, W.; Chang, Y.; Fu, D. Graphene oxide incorporated polypyrrole composite materials: optimizing the electropolymerization conditions for improved supercapacitive properties. *J. Mater. Sci. Mater. Electron.* **2019**, *30*, 1109−1116.
(69) Wu, T. M.; Lin, S. H. Synthesis, characterization, and electrical properties of polypyrrole/multiwalled carbon nanotube composites. *J. Polym. Sci., Part A: Polym. Chem.* **2006**, *44*, 6449−6457.
(70) Konwer, S.; Boruah, R.; Dolui, S. K. Studies on conducting polypyrrole/graphene oxide composites as supercapacitor electrode. *J. Electron. Mater.* **2011**, *40*, 2248−2255.
(71) Gómez-Navarro, C.; Weitz, R. T.; Bittner, A. M.; Scolari, M.; Mews, A.; Burghard, M.; Kern, K. Electronic transport properties of individual chemically reduced graphene oxide sheets. *Nano Lett.* **2007**, *7*, 3499−3503.

https://doi.org/10.1021/acsomega.2c03882
ACS Omega XXXX, XXX, XXX−XXX